Geostatistical Applications of Spartan Spatial Random Fields

S. N. Elogne and D. T. Hristopulos

Abstract Spartan Spatial Random Fields (SSRFs) were recently proposed (Hristopulos 2003) as a new method for modelling spatial dependence. This paper focuses on (i) the inference of Gaussian SSRF model parameters from spatial data using kernel methods and (ii) the identification of geometric anisotropy by means of the covariance tensor identity (CTI) method (Hristopulos 2002). The methods presented are illustrated with the help of synthetic data and a real set of elevation data. Kriging predictions obtained with the Spartan covariance estimator are compared to those obtained with standard estimators. Based on these results, the Spartan estimator provides a useful alterative to parametric covariance estimators, which it may outperform in certain cases.

1 Introduction

Spatial interpolation has many applications in the fields of the earth and environmental sciences. The widely used methodology is based on the kriging algorithm, which employs the spatial continuity structure encoded in the semivariogram or the covariance function. Estimation of the latter from the data is often conducted under the Gaussian and isotropic assumptions. Reliable estimation of the spatial structure is crucial to producing accurate kriging maps.

Here we investigate the problem of estimating the spatial continuity for both isotropic and anisotropic processes, in the framework of Spartan Spatial Random Fields (Hristopulos 2003). The Spartan Spatial Random Fields (SSRFs) aim to provide a versatile, formally and computationally efficient approach for modelling spatial dependence. The SSRFs possess a Gibbs joint probability density function (pdf) that is expressed in terms of physically motivated interactions between the fluctuations, i.e., $f\left[X_\lambda(\mathbf{s})\right] = Z^{-1}\exp\left\{-H\left[X_\lambda(\mathbf{s})\right]\right\}$, where Z is a normalization factor and the *energy functional* H embodies the interactions. The following functional will be used

S. N. Elogne
Department of Mineral Resources Engineering, Technical University of Crete,
Chania 73100, Greece
e-mail: elogne@mred.tuc.gr

A. Soares et al. (eds.), *geoENV VI – Geostatistics for Environmental Applications*, 477–487

$$H = \frac{1}{2\eta_0 \xi^d} \int d\mathbf{s} \Big[\big\{ X_\lambda(\mathbf{s}) - m_X(\mathbf{s}) \big\}^2 + \eta_1 \xi^2 \big\{ \nabla X_\lambda(\mathbf{s}) \big\}^2 + \xi^4 \big\{ \nabla^2 X_\lambda(\mathbf{s}) \big\}^2 \Big], \tag{1}$$

where $m_X(\mathbf{s}) = E\left[X_\lambda(\mathrm{s})\right]$. Equation (1) provides a class of flexible parametric models derived from the same functional. The three terms in the functional can be viewed as physical constraints related to the square of the fluctuations, as well as their gradient and curvature. Such terms can be either physically motivated or simply used as abstract constraints that lead to flexible covariance models.

The *SSRF parameters* include η_0 (the scale parameter), η_1 (the shape parameter), ξ (the characteristic length) and k_c(the frequency cutoff). The isotropic Spartan covariance spectral density is given by the following equation, where $\delta_{\| \mathbf{k} \| \le k_c} = 1$ for $\| \mathbf{k} \| \le k_c$ and 0 for $\| \mathbf{k} \| > k_c$:

$$\widetilde{G}_\lambda(\mathbf{k}) = \eta_0 \xi^d \delta_{\|\mathbf{k}\| \le k_c} \big/ \big(1 + \eta_1 \xi^2 \|\mathbf{k}\|^2 + \xi^4 \|\mathbf{k}\|^4\big). \tag{2}$$

Permissibility conditions follow simply from requiring non-negative values of the spectral density (Hristopulos 2003; Hristopulos & Elogne 2006).

The above covariance spectral density corresponds to differentiable *random fields* (RFs) for finite k_c and non-differentiable ones for infinite k_c (Hristopulos & Elogne 2006). An important issue for practitioners is the ability to differentiate between covariance models (Gorsich & Genton 2000). In the Spartan framework one can distinguish between models based on the values of the SSRF parameters. SSRF model inference is computationally efficient, because it requires the estimation of a small set of parameters (Hristopulos 2003).

This paper is organized as follows: Section 2 focuses on SSRF parameter inference using kernel methods. In Section 3, identification of anisotropic covariance models using the covariance tensor identity method is reviewed, and extensions based on kernel methods are introduced. Section 4 is devoted to the numerical investigations of the proposed methods using simulated data sets. Section 5 presents an application of the methods to real data. Finally, conclusions and some open issues for further research are presented in Section 6.

2 SSRF Parameter Inference

Parameter inference is based on matching sample (experimental) estimates for the variance as well as *generalized gradient and curvature constraints* with respective values of stochastic (model) constraints (Hristopulos 2003; Elogne & Hristopulos, 2006b). The stochastic constraints are as follows:

$$E[S_0] = G_\lambda(0), \quad E[S_1] = 2d\, F_\lambda(a_1) \big/ a_1^2, \tag{3}$$

$$E[S_2] = \Big\{ 8d^2 F_\lambda(a_2) - 4d(d-1) F_\lambda(a_2\sqrt{2}) - 2d F_\lambda(2a_2) \Big\} \Big/ a_2^4, \tag{4}$$

where d is the *spatial dimension*, F_λ the semivariogram, and a_1, a_2 isotropic spatial increments. Using the spectral representation of isotropic covariance models, the stochastic constraints are expressed in terms of one-dimensional integrals that involve the unknown SSRF parameters.

In order to define corresponding sample constraints, a *continuous*, *isotropic* and *compactly supported* kernel$K$ and two bandwidth parameters h_1 and h_2 are introduced. Kernel averages of the field quantities are denoted as follows:

$$\left\langle X_{i,j}^2 \right\rangle_h \equiv \sum_{i \neq j} \left\{ X(\mathbf{s}_i) - X(\mathbf{s}_j) \right\}^2 K\left((\mathbf{s}_i - \mathbf{s}_j)/h \right) \Bigg/ \sum_{i \neq j} K\left((\mathbf{s}_i - \mathbf{s}_j)/h \right). \tag{5}$$

If $\overline{\mu_X}$ is the sample mean, the sample constraints are given by

$$\overline{S_0} = \tfrac{1}{n} \sum_i \left\{ X(\mathbf{s}_i) - \overline{\mu_X} \right\}^2, \quad \overline{S_1} = d \left\langle X_{i,j}^2 \right\rangle_{h_1} \Big/ a_1^2, \tag{6}$$

$$\overline{S_2} = \left\{ 4d^2 \mu_1 \left\langle X_{i,j}^2 \right\rangle_{h_2} - 2d(d-1)\mu_2 \left\langle X_{i,j}^2 \right\rangle_{h_2\sqrt{2}} - d \left\langle X_{i,j}^2 \right\rangle_{2h_2} \right\} \Big/ a_2^4. \tag{7}$$

The increments a_1 and a_2 as well as μ_1 and μ_2, are functions of the sampling locations, selected so that the sample constraints are asymptotically unbiased estimators of the stochastic counterparts (Elogne & Hristopulos 2006b).

2.1 Bandwidth Selection

The choice of the bandwidth parameters is a crucial issue. Classical methods are based of minimizing some criterion (e.g., mean square error) which depends on unknown characteristics of the process, such as the true semivariogram model and its second derivative (Garcia-Soidan et al. 2004). In the Spartan framework, the bandwidths are determined from the *consistency principle* $a_p = \left\langle \left\| \mathrm{s}_i - \mathrm{s}_j \right\|^{2p} \right\rangle_{h_p}^{1/2p}$, for $p = 1, 2$ (Elogne & Hristopulos 2006b). Under mild regularity conditions on the sampling locations and the kernel, it is proved that $a_p = h_p \left(m_{K,p+1}/m_{K,1} \right)^{1/2p} + o(h_p)$ almost surely for $p = 1, 2$ in d= 2, where $m_{K,j}$ represent moments of the kernel function. Estimates of the increments a_1 and a_2 are derived from the neighbor distance distribution of the sampling network.

2.2 Constraints Fitting

Given the nonlinear dependence of the stochastic constraints, i.e., equations (6) and (7), on the SSRF parameters, the latter need to be determined numerically by solving a system of equations that fit the stochastic constraints to the sample constraints, given by equations (6) and (7). This is accomplished by minimizing a nonlinear *distance*

functional Φ, which measures the deviation between the sample and the stochastic constraints. The initial form of the functional given in (Hristopulos 2003) assumed a fixed cutoff frequency. The distance functional has been recently extended (Elogne & Hristopulos 2006b) to allow for direct inference of the cutoff from the data.

The minimization can be implemented using standard optimization algorithms, (e.g., the Nelder-Mead simplex search method). In the cases explored so far the convergence is very fast (for a sample of 100 locations approximately two seconds on a laptop with a Celeron M processor at 1.1GHz and 256Mb RAM, running Matlab under Windows XP; see also Hristopulos 2003). The initial values of the SSRF parameters, except for the shape coefficient, are not a crucial factor in the optimization results. In our experience, all the "solutions" to which the optimization converges lead to similar spatial dependence (covariance function), although sometimes different covariance estimators are obtained, some of which correspond to local minima of Φ (also see Section 4.2).

3 Anisotropy Identification

Spatial data often exhibit continuity properties that depend on the direction in space. Accurate kriging maps require a reliable description of the anisotropic model. Classical approaches for anisotropy estimation are based mostly on empirical methods (Goovaerts 1997). In the Spartan framework, it is possible to formulate the energy functional for general anisotropic dependence. However, this modification increases the number of model parameters: describing *geometric anisotropy* in two dimensions requires an anisotropy ratio ρ and an orientation angle ϕ. If these parameters are known, isotropic coordinate transformations can be applied to obtain a new system, in which the spatial distribution is *statistically isotropic*. The isotropic SSRF model can then be applied in the new system.

Systematic, unsupervised identification of anisotropy parameters, especially if it enables detection of sudden changes in the spatial distribution, is an important aspect of an automated mapping system for environmental monitoring and emergencies warning systems. The *covariance tensor identity* (CTI) approach allows estimating the anisotropic parameters (Hristopulos 2002), and in certain cases it provides explicit solutions for the anisotropic parameters (Hristopulos 2006). For second-order differentiable random fields, if Q_{11}, Q_{22} and Q_{12} denote the elements of the sample gradient tensor $Q_{ij} = \frac{1}{M}\sum_{m=1}^{M} \partial_i X(\mathbf{s}_m)\, \partial_j X(\mathbf{s}_m)$, it follows that

$$Q_{11} = \alpha_{\mathbf{x}} \left\{ \rho^2 \left[\sin\phi\right]^2 + \left[\cos\phi\right]^2 \right\}, \; Q_{22} = \alpha_{\mathbf{x}} \left\{ \rho^2 \left[\cos\phi\right]^2 + \left[\sin\phi\right]^2 \right\}$$
$$Q_{12} = \alpha_{\mathbf{x}} \left(1 - \rho^2\right) \sin\phi \cos\phi, \tag{8}$$

where the coefficient α_{x} is related to the covariance and is independent of ρ and ϕ. Using the *scaled gradient moments* $Z_g = Q_{22}/Q_{11}$ and $Z_f = Q_{12}/Q_{11}$ eliminates $\alpha_{\mathbf{x}}$, and the anisotropic parameter estimates are given by the following equations:

$$\widehat{\phi_{\pm}} = \tan^{-1}\left(\frac{Z_g - 1 \pm \sqrt{\Delta}}{2Z_f}\right) \text{ and } \widehat{\rho_{\pm}} = \left\{\frac{2\left(Z_g - 2Z_f^2 - 1 \pm \sqrt{\Delta}\right)}{\left(Z_g - 1 \pm \sqrt{\Delta}\right)\left(Z_g + 1 \pm \sqrt{\Delta}\right)}\right\}^{1/2}, \tag{9}$$

where $\Delta = (Z_g - 1)^2 + 4Z_f^2$ and the $+(-)$ signs correspond to equivalent solutions with ρ greater (smaller) than unity respectively.

In practice, finite differences are used to estimate the gradient tensor. For an increment b_j in the direction $\overrightarrow{\mathbf{e_j}}$, we define the following quantities in terms of the semivariogram F : $q_{11} = F\left(b_1\overrightarrow{\mathbf{e}_1}\right)$, $q_{22} = F\left(b_2\overrightarrow{\mathbf{e}_2}\right)$ and $q_{12} = F\left(b_1\overrightarrow{\mathbf{e}_1} - b_2\overrightarrow{\mathbf{e}_2}\right)$. We introduce two lag tolerances τ_1 and τ_2, a continuous, and compactly supported kernel K_1 that selects near neighbors in specified directions, and two smoothing parameters h_1 and h_2 (Elogne & Hristopulos 2006a). For conciseness we define $x_{ij} = x_i - x_j$, $y_{ij} = y_i - y_j$. The estimators $\overline{q_{ij}}$ of the q_{ij} are defined as follows:

$$\overline{q_{11}} = \frac{\sum_{i\neq j} K_1\left(x_{ij}/h_1\right)\delta_{|y_{ij}|\leq\tau_1} X_{ij}^2}{\sum_{i\neq j} K_1\left(x_{ij}/h_1\right)\delta_{|y_{ij}|\leq\tau_1}}, \quad \overline{q_{22}} = \frac{\sum_{i\neq j} K_1\left(y_{ij}/h_2\right)\delta_{|x_{ij}|\leq\tau_2} X_{ij}^2}{\sum_{i\neq j} K_1\left(y_{ij}/h_2\right)\delta_{|x_{ij}|\leq\tau_2}},$$
$$\overline{q_{12}} = \frac{\sum_{i\neq j} K_1\left(x_{ij}/h_1\right) K_1\left(y_{ij}/h_2\right)\delta_{x_{ij}\, y_{ij}<0} X_{ij}^2}{\sum_{i\neq j} K_1\left(x_{ij}/h_1\right) K_1\left(y_{ij}/h_2\right)\delta_{x_{ij}\, y_{ij}<0}}. \tag{10}$$

The increments b_j are estimated from kernel averages of the distances between sampling points in the respective directions. Bandwidths are linearly related to the increments with coefficients that depend on the kernel moments and follow from asymptotic analysis. The tolerances are taken proportional to the square root of the average area divided by the number of sampling points; the proportionality coefficients are selected to render the tolerance smaller than the bandwidth.

The CTI method allows checking the consistency of the anisotropy estimates by iterative application to the transformed coordinate system. Asymptotic analysis supports the statistical accuracy and reliability of the method.

4 Numerical Investigations

In this section numerical simulations are conducted to evaluate the performance of the methods presented above. The first experiment focuses on the estimation of isotropic spatial dependence from simulated data using an SSRF model. The second experiment concerns the identification of geometric anisotropy from a training data set and cross-validation of the results at a set of prediction points. The triangular kernel is used in all instances of kernel averaging. Unless otherwise specified, the *ordinary kriging* (OK) spatial interpolator is used. The maps are generated on 50×50 square grids.

4.1 First Experiment

One hundred independent samples of size $n = 50$ from a $N(0,1)$ (Gaussian, zero-mean, unit variance) RF are simulated using the Cholesky method on a square of side $L = 2$. The spherical, $\rho_s(||\mathbf{r}||) = \left\{1 - 3||\mathbf{r}||/2b_s + ||\mathbf{r}||^3/2b_s^3\right\}\delta_{||r||\leq b_s}$, and the exponential, $\rho_e(||\mathbf{r}||) = \exp(-||\mathbf{r}||/b_e)$, covariance models are used with b_s =0.5 and b_e =0.3. For each simulation, the SSRF model parameters are determined as discussed in Section 2. The covariance is calculated by inverting the spectral density (2), which requires an 1-d numerical integral (Hristopulos 2003).

The box plots of the Spartan covariance estimators are displayed in Figure 1 for ten distance lags, uniformly spaced between 0 and three correlation lengths. As shown in the plots, the Spartan estimator captures satisfactorily the spatial dependence of non differentiable processes.

4.2 Second Experiment

One sample of size $n = 400$ from an $N(20,10)$ RF ($m_X = 25$, $\sigma_X = 10$) is generated on a square domain of length $L = 10$. The hole-type covariance $\rho_h(||\mathbf{r}||) = b_h \sin(||\mathbf{r}||/b_h)/||\mathbf{r}||$ (in isotropic coordinates) with $b_h = 1$ and anisotropic parameters $\phi = 20^\circ$, $\rho = 2$ is used. The training set involves $n_{tr} = 100$ randomly selected points, and the prediction set the remaining $n_{pr} = 300$ points.

Figure 2 shows a map derived from all the data using nearest-neighbor interpolation as well as the locations of the training and prediction sets.

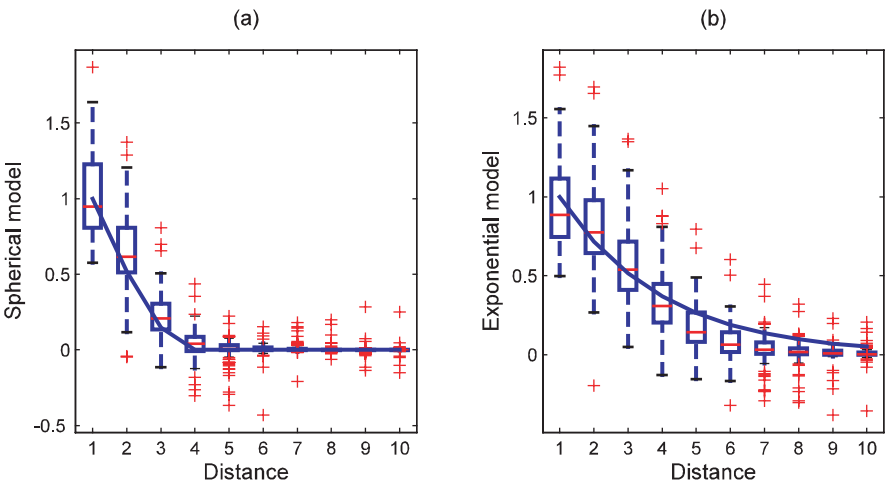

Fig. 1 Box-plots of the Spartan covariance estimator based on 100 independent samples drawn from random fields with spherical (a) and exponential (b) covariance functions, plotted against the theoretical covariances (continuous lines)

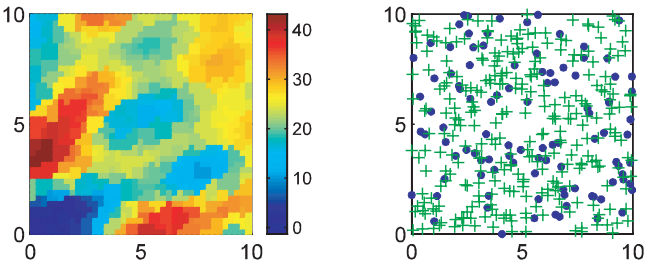

Fig. 2 (Left): Nearest-neighbor interpolation map; (right) Training location set (dots) and prediction location set (crosses)

4.2.1 Model Estimation Under the Isotropic Assumption

The training set data are modeled using the isotropic assumption. The experimental omnidirectional semivariogram is calculated and fitted with three parametric models (hole-type, exponential and spherical). In addition, two Spartan covariance estimators are obtained by constraint fitting. Initial values of η_1 in the range $[-0.5, 1.5]$ lead to the Spartan I model (η_0 =533.59, η_1 =0.56, ξ =0.66, k_c =2.41), while other initial values lead to the Spartan II model (η_0 =533.59, η_1 =1.80, ξ =0.99, k_c =6.51). The latter corresponds to a local minimum of the distance functional, while the Spartan I is the global minimum. Figure 3 displays a plot of the empirical semivariogram, as well as plots of the five estimators. The Spartan I estimator displays an oscillatory dependence, which is also present in the hole-type model used to generate the data. In contrast, the Spartan II model approaches monotonically the sill.

OK predictions are derived at the 300 prediction points and compared with the "actual" values. Table 1 summarizes the performance of the five models, based on the *mean error* (ME), *mean absolute error* (MAE), *root mean square error* (RMSE) and the Pearson *correlation coefficient* (R^2).

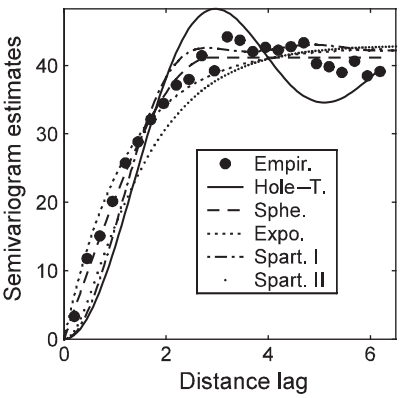

Fig. 3 Plots of the experimental semivariogram and five different isotropic estimators

Table 1 OK cross validation results (isotropic assumption)

	ME	MAE	RMSE	R^2
Spherical	0.98	2.13	3.38	0.90
Exponential	0.99	2.19	3.43	0.90
Hole-Type	1.04	2.99	4.06	0.87
Spartan I	1.00	1.90	3.28	0.91
Spartan II	0.97	2.00	3.31	0.91

All the estimators tested perform similarly with respect to the measures of the Table 1. The hole-type estimator is marginally worse. This may be due partly to the sampling density of the training set not being sufficient to accurately estimate the anti-correlations of the hole-type model. The Spartan I estimator's milder oscillations are in better agreement with the empirical semivariogram than the hole-type estimator. This is probably due to the flexibility provided by the SSRF shape coefficient. The Spartan I estimator has slightly lower MAE and RMSE values than the other estimators, but it gives a marginally higher ME. The R^2values are practically the same for all estimators except for the hole-type.

4.2.2 Model Estimation with Anisotropy Detection

Based on the 100 observations of the training set, the anisotropic parameters obtained by the CTI method are $\widehat{\phi}$=28.75° and $\widehat{\rho}$= 1.71. For comparison, if all 400 locations were used, $\widehat{\phi}$=26.59° and $\widehat{\rho}$=1.76. The increments are equal to $h_1 = 2.20$, $h_2 = 2.08$, and the tolerances are set to $\delta_j = h_j/4$, for $j = 1, 2$. Transformation in the isotropic coordinate system follows (applying CTI in this system yields $\widehat{\phi} = -21.00°$ and $\widehat{\rho}$=1.17).

The spatial dependence is modeled in the isotropic system. The resulting estimators outperform the isotropic counterparts (see Table 2). The hole-type estimator is not shown, because it performs considerably worse than the others. In both the isotropic and anisotropic cases, the Spartan I covariance outperforms the other models, but its advantage is sharpened after the anisotropic correction.

Figure 4 displays the kriging maps obtained with the Spartan I (plot a) and the spherical (plot b) estimators. The spherical model underestimates higher values as evidenced by the ranges of the kriging maps (also compare with Figure 2).

Table 2 OK cross validation results (anisotropic assumption)

	ME	MAE	RMSE	R^2
Spherical	0.85	1.92	2.90	0.94
Exponential	0.87	1.97	2.94	0.94
Spartan I	0.78	1.64	2.72	0.95
Spartan II	0.82	1.78	2.80	0.95

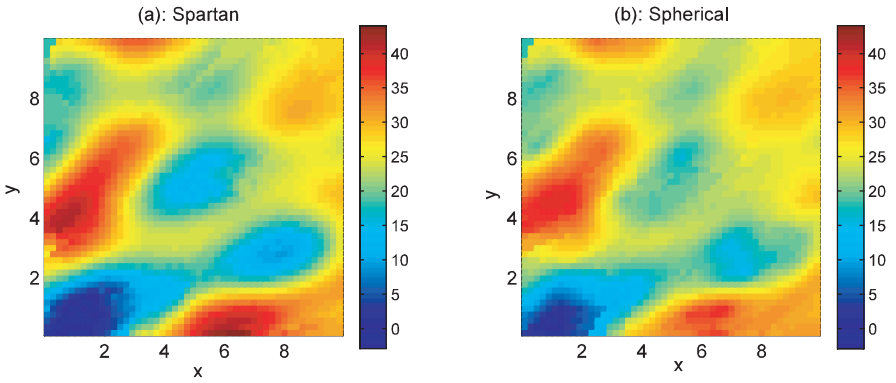

Fig. 4 OK maps obtained with (a) Spartan I and (b) spherical covariance models

5 Application to Elevation Data

We consider a set of elevation data (sample size n= 52), available online at http://www.maths.lancs.ac.uk/∼diggle to illustrate the performance of CTI and the SSRF covariance. CTI application gives $\widehat{\rho}$ =1.03 and $\widehat{\phi}$ =33.11° with tolerances taken equal to 25% of the increments. Hence, there is no significant anisotropy.

Next, we perform leave-one-out cross-validation using the Spartan covariance, as well as parametric (spherical, exponential, hole-type, Gaussian and power-law) estimators. The SSRF method yields a single covariance estimator regardless of the initial value of η_1. The best cross-validation results are obtained with the hole-type covariance, but a kriging map based on this model is physically unsatisfactory (it includes negative values). The spherical and the exponential parametric estimators perform also poorly. The Gaussian and SSRF estimators exhibit the best performance as summarized in the Table 3:

The semivariograms (empirical and four estimators) are presented in Fig. 5 (left plot), with the elevation map obtained using the SSRF estimator (right plot). The SSRF estimator misses the clearly non-stationary long-range dependence of the empirical semivariogram, which is either due to mean non-stationarity or long-range fluctuations. Yet, cross validation produces reasonable errors (e.g., mean absolute relative error around 6%). This is due to the greater importance of short-range neighbours in spatial interpolation and the ability of ordinary kriging to capture slowly-changing non-stationarities of the mean.

Table 3 Leave-one-out cross validation OK performance

	ME	MAE	RMSE	MARE	RMSRE	R^2
Gaussian	5.82	53.18	60.85	0.06	0.07	0.39
Spartan	5.17	53.07	60.67	0.06	0.07	0.39

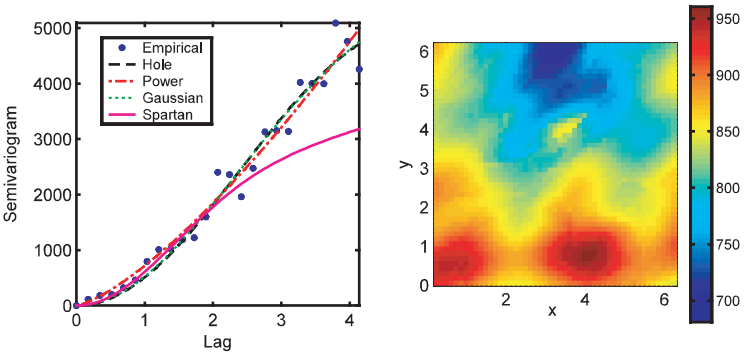

Fig. 5 Elevation semivariograms (left) and OK map based on the SSRF model (right)

6 Conclusions

We present an overview of the SSRF approach, and we investigate its performance by means of simulated and real data. The central idea of the SSRF approach is to use interactions between the field values to model spatial correlations. This viewpoint leads to methodological departures from classical geostatistics, having implications for both *model inference* and *spatial prediction*. Regarding parameter inference, an important advantage of the SSRF approach is the ability to determine the spatial dependence with minimal user involvement.

We also study the application of the CTI method, which is a promising tool for the *automatic detection* of anisotropy, using kernels to estimate the sample averages. The current formulation is based on differentiable covariance models, but extensions to non-differentiable cases are being investigated.

Acknowledgments This research is supported by a Marie Curie Transfer of Knowledge Fellowship (Project SPATSTAT, No. MTKD-CT-2004-014135), and co-funded by the European Social Fund and National Resources – (EPEAEK-II) PYTHAGORAS.

References

Elogne S, Hristopulos D (2006a) Kernel methods for estimating anisotropic parameters by means of the covariance tensor identity. Geophys Res Abstr vol 8, 02170

Elogne S, Hristopulos D (2006b) On the inference of spatial continuity using Spartan random field models, www.arXiv:math.ST/0603430

Garcia-Soidan P, Febrero-Bande M, Gonzalez-Manteiga (2004) Non-parametric kernel estimation of an isotropic semivariogram. J Stat Plan Infer 121:65–92

Goovaerts P (1997) Geostatistics for natural resources evaluation. Oxford, New York

Gorsich D, Genton M (2000) Variogram model selection via non-parametric derivative estimation. Math Geol 27:249–270

Hristopulos D (2002) New anisotropic covariance models and estimation of anisotropic parameters based on the covariance tensor identity. Stoch Env Res Risk A 16:43–62

Hristopulos D (2003) Spartan Gibbs random field models for geostatistical applications. SIAM J Sci Comput 24:2125–2162

Hristopulos D (2006) Identification of spatial anisotropy by means of the covariance tensor identity. In: Dubois (ed) GEUR 21595 EN - Automatic Mapping Algorithms for Routine and Emergency Monitoring Data, Office for Official Publications of the European Communities, Luxembourg, ISBN 92-894-9400-X, pp 103–124

Hristopulos D, Elogne S (2006) Analytic properties and covariance functions of a new class of generalized Gibbs random fields. IEEE T Inform Theory forthcoming (Dec. 2007). Preprint online at: http://arxiv.org/abs/cs.IT/0605073